1 Model description

HadCM3 model has been used extensively for studies of the Pliocene climate within the Pliocene Model Intercomparison Project [1-4]. HadCM3 consists of two main components: an atmospheric component (HadAM3) and an oceanic component (HadOM3) [5-7]. The horizontal resolution of the atmosphere model is 2.5° in latitude by 3.75° in longitude and consists of 19 layers in the vertical. The atmospheric model has a time step of 30 min and includes a radiation scheme that can represent the effects of major and minor trace gases [8]. The HadOM3 spatial resolution of the ocean is horizontal 1.25° by 1.25° and vertical 20 layers. The fact that the HadCM3 consistently performs well in tests against other coupled atmosphere–ocean models [9,10] increases our confidence in its palaeoclimate simulations.

2 Detail boundary conditions

As abundant geological data are available and explicit boundary conditions have been designed for the middle part of the Piacenzian Stage of the Pliocene (3.264 to 3.025 Ma), which is also referred to as the mid-Pliocene Warm Period (mPWP), many paleoclimate simulations targeting this time slice have been conducted [11-14]. For this study, we also focus on the mPWP time slice, for which the required mid-Pliocene boundary conditions were supplied by the dataset of U.S. Geological Survey Pliocene Research Interpretations and Synoptic Mapping Group's (PRISM3D) dataset [15]. This dataset includes topography and bathymetry, coastlines, land surface properties (i.e., vegetation, soil type, and ice sheet coverage) and atmospheric composition with respect to pre-industrial conditions. The Greenland Ice Sheet and the West Antarctic Ice Sheet, which currently store ~13 m sea-level equivalent ice [10,16], are thought to have largely melted during the mid-Pliocene warm period [17,18]. The mid-Pliocene atmospheric CO_2 concentration was set to 405 ppmv. All other trace gases were specified at pre-industrial concentrations [2]. The realistic simulation of the modern climate by HadCM3 makes it a good candidate for investigating the response of climate to orbital forcing.

3 Changes of shortwave incoming solar radiation

On an annual mean basis, the shift in obliquity from minimum to maximum values slightly decreases the insolation at the equator by about 4 W/m^2; however, it causes a much larger increase at the poles by 16 W/m^2 (Fig. S1a). The zonally averaged temperature changes induced by obliquity (Fig. 2b in the manuscript) is consistent with the insolation changes. The change in precession from aphelion to perihelion results in no change of the zonally averaged annual mean insolation (Fig. S1b), which is consistent with the smallest effect of precession changes on temperature. For variation in eccentricity, the simulated annual mean shortwave incoming solar radiation results demonstrate nearly pervasive increase over the globe ((~1–3 W/m^2; Fig. S1c), which is consistent with the extensive warming over the globe.

The precipitation responses occur mostly in the tropical regions (Fig. 2g–l in the manuscript), which is climatically dominated by the ITCZ. Previous studies have demonstrated that global temperature change may increase the interhemispheric temperature contrast, thus leading to a shift of ITCZ to the warmer hemisphere [19]. Although the obliquity has the most effect on temperature, the temperature increases significantly both in the northern and southern high latitudes, which essentially does not change the interhemispheric temperature contrast. However, for precession changes, the temperature decreases at northern high latitudes and increases at the southern high latitudes, leading to a large interhemispheric temperature contrast and an associated ITCZ shift. Therefore, precession change has the most effect on the precipitation at low latitudes.

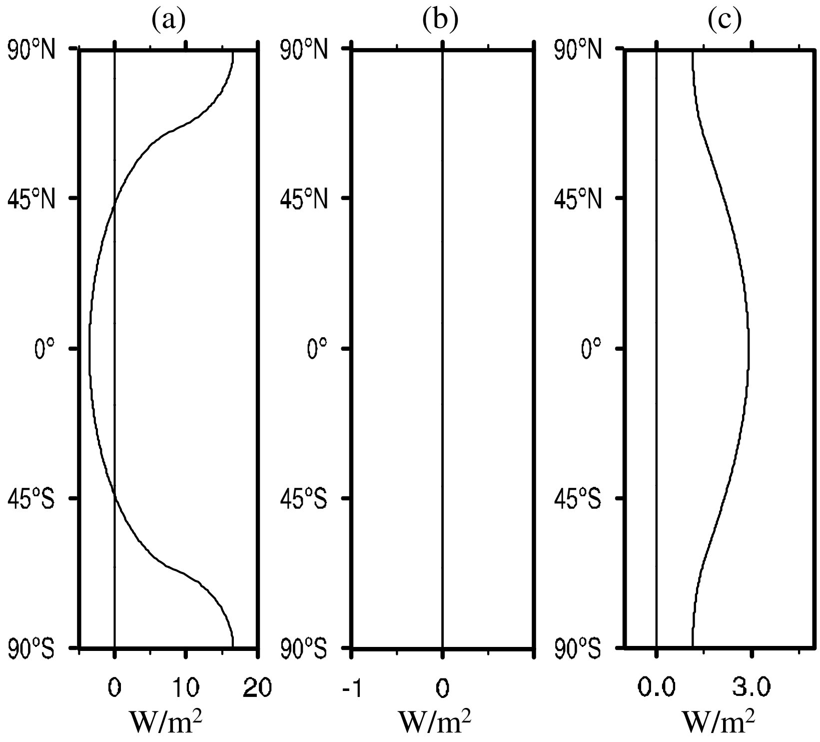

Fig. S1. Zonally averaged annual mean changes of short wave (SW) incoming solar radiation at the TOA (W/m^2) between (a) $E_{\max}P_{\max}O_{\max}$ and $E_{\max}P_{\max}O_{\min}$, (b) $E_{\max}P_{\min}O_{\min}$ and $E_{\max}P_{\max}O_{\min}$, and (c) $E_{\max}P_{\max}O_{\min}$ and $E_{\min}P_{\max}O_{\min}$.

Table S1 *Localities and data used in the reconstruction of the Pliocene paleoclimate*

No.	Site	Location	Proxy data	Periodicity signal	References
1	U1338	2.51°N, 117.97°W	Benthic $\delta^{18}O$	Obliquity	[20]
2	ODP 982	57.5°N, 15.87°W	Benthic $\delta^{18}O$; Alkenone	Obliquity	[20,21]
3	ODP 659	18.08°N, 21.03°W	Benthic $\delta^{18}O$	Obliquity	[22]
4	U1313	41°N, 32.57°W	Plant leaf wax	Obliquity	[23]
5	ODP 607	41°N, 33°W	Mg/Ca in fossil ostracodes	Obliquity	[21,24,25]
6	ODP 609	50°N, 24°W	Benthic $\delta^{18}O$	Obliquity	[26]
7	AND-1B	77.89°S, 167.09°E	Sedimentation succession; Diatom	Obliquity	[18,27,28]

			assemblages		
8	U1208	36.13°N, 158.2°E	Alkenone; Benthic $\delta^{18}O$	Obliquity	[29-31]
9	U911	80.5°N, 8.2°E	Total organic carbon	Obliquity	[32]
10	Wujiamao	37.25°N, 110.05°E	Magnetic susceptibility	Obliquity	[33]
11	U1143	9.37°N, 113.28°E	Benthic $\delta^{18}O$	Obliquity	[25]
12	U846	3.095°S, 90.82°W	Benthic $\delta^{18}O$	Obliquity	[34,35]
13	U849	0.18°N, 110.52°W	Benthic $\delta^{18}O$, $\delta^{13}C$	Obliquity	[36]
14	U610	53°N, 19°W	Ostracode assemblages	Obliquity	[37]
15	Dawson	64.1°N, 139.2°W	IRD	Obliquity	[38]
16	U1448	10.63°N, 93°E	Benthic and planktic foraminiferal $\delta^{18}O$, $\delta^{13}C$	Obliquity	[39]
17	U552	56°N, 23°W	*Discoaster* abundance	Obliquity	[40]
18	U798	37.63°N, 134.8°E	Sedimentation rates	Obliquity	[41]
19	El'gygytgyn	67.5°N, 172.08°E	Rb/Sr ratio	Obliquity	[42]
20	Tiburon	23.29°S, 70.49°W	Sedimentology and sequence stratigraphy	Obliquity	[43]
21	Yabuta	3713°N, 6.35°E	Molluscs, diatoms, and ostracodes	Obliquity	[44]
22	U1146	19.45°N, 116.27°E	Benthic $\delta^{18}O$	Obliquity	[25]
23	U548	48.92°N, 12.16°W	Benthic $\delta^{18}O$	Obliquity	[45]
24	U1478	25.82°S, 34.77°E	Leaf waxes δD_{wax}	Obliquity	[46]
25	Huatugou	38.5°N, 91.92°E	Magnetic susceptibility	Precession	[47]
26	Orogen	32°N, 82°E	lacustrine carbonate $\delta^{18}O$	Precession	[48]
27	Spertivento	38°N, 16°E	Organic carbon content	Precession	[49]
28	ODP 964	36.26°N, 17.75°E	Chemical composition	Precession	[50,51]
29	ODP 967	34.07°N,	Chemical composition;	Precession	[50,52,53]

		32.73°E	Aeolian dust		
30	ODP 969	33.84°N, 24.88°E	Chemical composition	Precession	[50]
31	Ptolemais	40.5°N, 21.65°E	Pollen; Sedimentary rhythmic alternations	Precession	[54-56]
32	Punta Piccola	37.3°N, 13.5°E	Planktonic $\delta^{18}O$; Biogenic compositions	Precession	[51,57-60]
33	Cape Spertivento	37.95°N, 16°E	Planktonic $\delta^{18}O$; Biogenic compositions	Precession	[57,59]
34	Maar Lake	41.83°N, 2.8°E	Pollen	Precession	[61]
35	Fiumana	44.15°N, 11.99°E	Paleoproductivity	Precession	[62]
36	Omo Group	3.5°N, 36.5°E	$\delta^{18}O$ of pedogenic carbonate	Precession	[63]
37	BTB13	0.55°N, 35.93°E	Leaf wax $\delta^{13}C_{wax}$	Precession	[64]
38	Monte Singa	38.5°N, 17°E	Mineralogical content	Precession	[51]
39	Vrica	39°N, 17.45°E	Mineralogical content	Precession	[51]
40	ODP 231	11.89°N, 48.25°E	Biomarker	Precession	[65]
41	Capo Rossello	37.47°N, 13.72°E	Planktonic foraminiferal assemblages	Precession	[57,66,67]
42	ODP 653	40.18°N, 12.19°E	Planktonic foraminiferal assemblages	Precession	[57]
43	ODP 661	9.45°N, 19.39°W	Eolian dust	Precession	[68,69]
44	ODP 662/663	1.39°S, 11.74°W	Eolian dust	Precession	[68,69]
45	ODP 664	0.11°N, 23.22°W	Eolian dust	Precession	[68,69]
46	ODP 721/722	16.62°N, 59.8°E	Eolian dust	Precession	[68,69]
47	Shilou	36.92°N, 110.93°E	Al/Na, Rb/Sr, and lightness	Eccentricity	[70]
48	Liulin	37.35°N, 110.75°E	Magnetic susceptibility	Eccentricity	[71]
49	Lupoaia	45.57°N, 26.92°E	Lithological cycles	Eccentricity	[72]
50	Huatugou	38.3°N, 91.26°E	Evaporite minerals	Eccentricity	[73]
51	U594	45.52°S,	Benthic $\delta^{18}O$, $\delta^{13}C$	Eccentricity	[74]

		174.95°E			
52	U1125	42.55°S, 178.17°W	Benthic $\delta^{18}O$, $\delta^{13}C$	Eccentricity	[74]
53	Changgoucun	34.3°N, 109.5°E	Grain size	Precession and Eccentricity	[75]
54	Lupoaia	44.8°N, 22.97°E	Pollen	Precession and Eccentricity	[76]
55	PL02	38.92°N, 106.6°E	Pollen; Magnetic susceptibility; Mean grains size	Precession and Obliquity	[77]
56	Dongwan	34.97°N, 105.78°E	Snail	Precession and Obliquity	[78]
57	U1359	64.9°S, 143.96°E	Mass accumulation rate	Precession and Obliquity	[79]
58	Makapansgat Valley	24.13°S, 29.18°E	Stable $\delta^{18}O$ and $\delta^{13}C$ of speleothems	Precession and Obliquity	[80]
59	U659	18.08°N, 21.03°W	Benthic $\delta^{18}O$; Dust flux	Precession and Obliquity	[22,68,69]
60	U925	4.2°N, 43.48°W	Magnetic susceptibility	Precession and Obliquity	[81]
61	U926	3.7°N, 42.9°W	Magnetic susceptibility	Precession and Obliquity	[81]
62	U927	5.5°N, 44.5°W	Magnetic susceptibility	Precession and Obliquity	[81]
63	U928	5.5°N, 44.8°W	Magnetic susceptibility	Precession and Obliquity	[81]
64	U929	5.98°N, 43.74°W	Magnetic susceptibility	Precession and Obliquity	[81]
65	U806	0.319°N, 159.36°E	Foraminiferal Mg/Ca and planktonic $\delta^{18}O$	Precession and Obliquity	[82,83]
66	VA	40.62°N, 0.98°W	Magnetic parameters	Precession and Obliquity	[84]
67	Wanganui	39.93°S, 175.05°E	Benthic $\delta^{18}O$; Relative sea-level	Precession and Obliquity	[85-87]
68	SG-1B	38.35°N, 92.27°E	Rb/Sr ratio; Grain size	Precession and Obliquity	[88]
69	XK-1	16.35°N, 120.35°E	Biogenic reef and carbonate deposition	Precession, Eccentricity, and Obliquity	[89]
70	Lingtai	35.07°N, 107.65°E	Grain size; Magnetic susceptibility	Precession, Eccentricity, and Obliquity	[90]
71	Zhaojiachun	35.75°N, 107.82°E	Grain size; Magnetic susceptibility	Precession, Eccentricity,	[90]

				and Obliquity	
72	Bojizhuang	34.53°N, 107.11°E	Grain size; Magnetic susceptibility; Carbonate content	Precession, Eccentricity, and Obliquity	[91]
73	Xiaoshuizi	35.81°N, 103.86°E	Grain size; Magnetic susceptibility; Carbonate content	Precession, Eccentricity, and Obliquity	[92]
74	U1361	64.41°S, 143.89°E	Iceberg-rafted debris mass accumulation rates	Precession, Eccentricity, and Obliquity	[93]
75	Xifeng	42.73°N, 124.72°E	Grain size; Magnetic susceptibility	Precession, Eccentricity, and Obliquity	[94]
76	642B	67.22°N, 2.93°E	Pollen	Precession, Eccentricity, and Obliquity	[95]

References

[1] Haywood AM, Dowsett HJ, Otto-Bliesner B, et al. Pliocene Model Intercomparison Project (PlioMIP): experimental design and boundary conditions (Experiment 1). Geosci Model Dev 2010; 3: 227–242.

[2] Haywood AM, Dowsett HJ, Robinson MM, et al. Pliocene Model Intercomparison Project (PlioMIP): experimental design and boundary conditions (Experiment 2). Geosci Model Dev 2011; 4: 571–577. doi:10.5194/gmd-4-571-2011.

[3] Bragg FJ, Lunt DJ, Haywood AM. Mid-Pliocene climate modelled using the UK Hadley Centre Model: PlioMIP Experiments 1 and 2. Geosci Model Dev 2012; 5: 1109–1125.

[4] Hunter SJ, Haywood AM, Dolan AM, et al. The HadCM3 contribution to PlioMIP phase 2. Clim Past 2019; 15(5): 1691–1713.

[5] Gordon C, Cooper C, Senior CA, et al. The simulation of SST, sea ice extents and ocean heat transports in a version of the Hadley Centre coupled model without flux adjustments. Clim Dynam 2000: 16(2): 147–168.

[6] Pope VD, Gallani ML, Rowntree PR, et al. The impact of new physical

parametrizations in the Hadley Centre climate model: HadAM3. Clim Dynam 2000; 16(2–3): 123–146.

[7] Valdes PJ, Armstrong E, Badger MPS, et al. The BRIDGE HadCM3 family of climate models: HadCM3@Bristol v1.0. Geosci Model Dev 2017; 10: 3715–3743.

[8] Edwards JM, Slingo A. Studies with a flexible new radiation code. I: Choosing a configuration for a large-scale model. Q J R Meteorol Soc 1996; 122(531): 689–719.

[9] Hegerl GC, Zwiers FW, Braconnot P, et al. Understanding and attributing climate change. In: Solomon S, Qin D, Manning M, et al. Climate Change 2007: The Physical Science Basis, Contribution of Working Group I to the Fourth Assessment Report of the Intergovernmental Panel on Climate Change. Cambridge University Press, Cambridge, United Kingdom, 2007.

[10] Dolan AM, Haywood AM, Hill DJ, et al. Sensitivity of Pliocene ice sheets to orbital forcing. Palaeogeogr Palaeoecl 2011; 309: 98–110,

[11] Jiang D, Wang H, Ding Z, et al. Modeling the middle Pliocene climate with a global atmospheric general circulation model. J Geophys Res 2005; 110: D14107.

[12] Kamae Y, Ueda H, Kitoh A. Hadley and Walker circulations in the mid-Pliocene warm period simulated by an atmospheric general circulation model. J Meteorol Soc Japan 2011; 89(5): 475–493.

[13] Zhang Z, Yan Q. Pre-industrial and mid-Pliocene simulations with NorESM-L: AGCM simulations. Geosci Model Dev 2012; 5: 1033–1043.

[14] Haywood AM, Hill DJ, Dolan AM, et al. Large-scale features of Pliocene climate: results from the Pliocene Model Intercomparison Project. Clim Past 2013; 9(1): 191–209.

[15] Dowsett HJ, Robinson M, Haywood AM, et al. The PRISM3D paleoenvironmental reconstruction. Stratigraphy 2010; 7: 123–139.

[16] Yamane M, Yokoyama Y, Abe-Ouchi A, et al. Exposure age and ice-sheet model constraints on Pliocene East Antarctic ice sheet dynamics. Nat Commun 2015;

6(1): 1–8,

[17] Lunt DJ, Foster GL, Haywood AM, et al. Late Pliocene Greenland glaciation controlled by a decline in atmospheric CO2 levels. Nature 2008; 454(7208): 1102–1105.

[18] Naish T, Powell R, Levy R, et al. Obliquity-paced Pliocene West Antarctic ice sheet oscillations. Nature 2009; 458(7236): 322–328.

[19] Broecker WS, Putnam AE. Hydrologic impacts of past shifts of Earth's thermal equator offer insight into those to be produced by fossil fuel CO2. Proc Natl Acad Sci USA 2013; 110(42):16710–16715.

[20] Drury AJ, John CM, Shevenell AE. Evaluating climatic response to external radiative forcing during the late Miocene to early Pliocene: New perspectives from eastern equatorial Pacific (IODP U1338) and North Atlantic (ODP 982) locations. Paleoceanography 2016; 31(1): 167–184.

[21] Lawrence KT, Herbert TD, Brown CM, et al. High-amplitude variations in North Atlantic Sea surface temperature during the early Pliocene warm period. Paleoceanography 2009; 24(2): PA2218.

[22] Tiedemann R, Sarnthein M, Shackleton NJ. Astronomic timescale for the Pliocene Atlantic $\delta^{18}O$ and dust flux records of Ocean Drilling Program Site 659. Paleoceanography 1994; 9(4): 619–638.

[23] Naafs BDA, Hefter J, Acton G, et al. Strengthening of North American dust sources during the late Pliocene (2.7 Ma). Earth Planet Sci Lett 2012; 317: 8–19.

[24] Dwyer GS, Cronin TM, Baker PA, et al. North Atlantic deepwater temperature change during late Pliocene and late Quaternary climatic cycles. Science 1995; 270(5240): 1347–1351.

[25] Tian J. Coherent variations of the obliquity components in global ice volume and ocean carbon reservoir over the past 5 Ma. Sci. China Earth Sci. 2013. 56(12), 2160–2172.

[26] Raymo ME, Ruddiman WF, Backman J, et al. Late Pliocene variation in Northern Hemisphere ice sheets and North Atlantic deep water circulation. Paleoceanography 1989; 4(4): 413–446.

[27] Konfirst MA, Scherer RP. Low amplitude obliquity changes during the early Pliocene reflected in diatom fragmentation patterns in the ANDRILL AND-1B core. Mar Micropaleontol 2012; 82: 46–52.

[28] Wilson GS, Levy RH, Naish TR, et al. Neogene tectonic and climatic evolution of the Western Ross Sea, Antarctica—Chronology of events from the AND-1B drill hole. Glob Planet Change 2012; 96: 189–203.

[29] Venti NL, Billups K. Stable-isotope stratigraphy of the Pliocene–Pleistocene climate transition in the northwestern subtropical Pacific. Palaeogeogr Palaeoclimatol Palaeoecol 2012; 326: 54–65.

[30] Venti NL, Billups K, Herbert TD. Increased sensitivity of the Plio-Pleistocene northwest Pacific to obliquity forcing. Earth Planet Sci Lett 2013; 384: 121–131.

[31] Venti NL, Billups K, Herbert TD. Paleoproductivity in the northwestern Pacific Ocean during the Pliocene-Pleistocene climate transition (3.0–1.8 Ma). Paleoceanography 2017; 32(2): 92–103.

[32] Knies J, Matthießen J, Vogt C, et al. Evidence of 'Mid-Pliocene (~3 Ma) global warmth' in the eastern Arctic Ocean and implications for the Svalbard/Barents Sea ice sheet during the late Pliocene and early Pleistocene (~3–1.7 Ma). Boreas 2002; 31(1): 82–93.

[33] Zhang H, Nie J, Liu X, et al. Spatially variable provenance of the Chinese Loess Plateau. Geology 2021; 49: 1155–1159.

[34] Shackleton NJ, Hall MA, Pate D. Pliocene stable isotope stratigraphy of Site 846. In Proc. Ocean Drill Program Sci Results 1995; 138: 337–355.

[35] Lawrence KT, Liu Z, Herbert TD. Evolution of the eastern tropical Pacific through Plio-Pleistocene glaciation. Science 2006; 312(5770): 79–83.

[36] Mix AC, Pisias NG, Rugh W, et al. Benthic foraminifer stable isotope record from Site 849 (0-5 Ma): Local and global climate changes. In Proc Ocean Drill Program Sci Results 1995; 138: 371–412.

[37] Cronin TM, Raymo ME, Kyle KP. Pliocene (3.2–2.4 Ma) ostracode faunal cycles and deep ocean circulation, North Atlantic Ocean. Geology 1996; 24(8): 695–698.

[38] Hidy AJ, Gosse JC, Froese DG, et al. A latest Pliocene age for the earliest and most extensive Cordilleran Ice Sheet in northwestern Canada. Quat Sci Rev 2013; 61: 77–84.

[39] Jöhnck J, Kuhnt W, Holbourn A, et al. Variability of the Indian Monsoon in the Andaman Sea across the Miocene-Pliocene transition. Paleoceanogr Paleoclimatol 2020; 35(9): e2020PA003923.

[40] Backman J, Hermelin O, Pestiaux P, et al. Palaeoclimatic and palaeoceanographic development in the Pliocene North Atlantic: Discoaster accumulation and coarse fraction data. Geol Soc London-Spec Publ 1986; 21(1): 231–242.

[41] deMenocal PB, Bristow JF, Stein R. Paleoclimatic applications of downhole logs: Pliocene-Pleistocene results from Hole 798B, Sea of Japan. In Proc Ocean Drill Program Sci Results 1992; 127: 393–407.

[42] Wennrich V, Minyuk PS, Borkhodoev V, et al. Pliocene to Pleistocene climate and environmental history of Lake El'gygytgyn, Far East Russian Arctic, based on high-resolution inorganic geochemistry data. Clim Past 2014; 10(4): 1381–1399.

[43] Tapia C, Wilson G, Ishman S, et al. Chronology, correlation and variability in Pliocene Glacioeustatic Cyclicites, Tiburon Basin, Mejillones Peninsula, Chile. Santiago 2009; 22: S10_038.

[44] Cronin TM, Kitamura A, Ikeya N, et al. Late Pliocene climate change 3.4–2.3 Ma: paleoceanographic record from the Yabuta Formation, Sea of Japan. Palaeogeogr Palaeoclimatol Palaeoecol 1994; 108(3–4): 437–455.

[45] Loubere P, Moss K. Late Pliocene climatic change and the onset of Northern Hemisphere glaciation as recorded in the northeast Atlantic Ocean. Geol Soc Am Bull 1986; 97(7): 818–828.

[46] Taylor AK, Berke MA, Castañeda IS, et al. Plio-pleistocene continental hydroclimate and Indian Ocean sea surface temperatures at the Southeast African Margin. Paleoceanogr Paleoclimatol 2021; 36(3): e2020PA004186.

[47] Su Q, Nie J, Luo Z, et al. Detection of strong precession cycles from the late

Pliocene sedimentary records of northeastern Tibetan Plateau. Geochem. Geophys Geosystems 2019; 20(8): 3901–3912.

[48] Saadeh CM, Saylor JE, Nie J, et al. Orbital forcing of late Miocene–early Pleistocene environmental change in the Zhada Basin, SW Tibetan Plateau. Paleoceanogr Paleoclimatol 2020; 35(8): e2019PA003781.

[49] Huang EQ, Tian J. Early Pliocene Precession Rhythm of African Monsoon and Mediterranean Sea Surface Productivity. Earth Sci J China Univ Geosci 2007; 32(3): 313–321.

[50] Brumsack HJ, Wehausen R. A geochemical record of precession-induced cyclic eastern Mediterranean sedimentation: implications for northern Sahara humidity during the Pliocene. Naturwiss 1999; 86(6): 281–286.

[51] Foucault A, Mélières F. Palaeoclimatic cyclicity in central Mediterranean Pliocene sediments: the mineralogical signal. Palaeogeogr Palaeoclimatol Palaeoecol 2000; 158(3–4): 311–323.

[52] Larrasoaña JC, Roberts AP, Rohling EJ, et al. Three million years of monsoon variability over the northern Sahara. Clim Dynam 2003; 21(7): 689–698.

[53] Grant KM, Rohling EJ, Westerhold T, et al. A 3 million year index for North African humidity/aridity and the implication of potential pan-African Humid periods. Quat Sci Rev 2017; 171: 100–118.

[54] Steenbrink J, Hilgen FJ, Krijgsman W, et al. Late Miocene to Early Pliocene depositional history of the intramontane Florina–Ptolemais–Servia Basin, NW Greece: Interplay between orbital forcing and tectonics. Palaeogeogr Palaeoclimatol Palaeoecol 2006; 238(1–4): 151–178.

[55] Steenbrink J, Kloosterboer-van Hoeve ML, Hilgen FJ. Millennial-scale climate variations recorded in Early Pliocene colour reflectance time series from the lacustrine Ptolemais Basin (NW Greece). Glob Planet Change 2003; 36(1–2): 47–75.

[56] Kloosterboer-van Hoeve ML, Steenbrink J, Visscher H, et al. Millennial-scale climatic cycles in the Early Pliocene pollen record of Ptolemais, northern Greece. Palaeogeogr Palaeoclimatol Palaeoecol 2006; 229(4): 321–334.

[57] Sprovieri R. Mediterranean Pliocene biochronology: A high resolution record based on quantitative planktonic foraminifera distribution. Riv Ital Paleontol S 1992; 98(1): 61–100.

[58] Nebout NC, Foucault A, Mélières F. Vegetation markers of palaeoclimate cyclical changes in the Pliocene of Punta Piccola (Sicily, Italy). Palaeogeogr Palaeoclimatol Palaeoecol 2004; 214(1–2): 55–66.

[59] Ding XH, Wang RJ, Jian-Ru LI, et al. The paleoproductivity forced by earth orbital forcing in Italy during early Pliocene. Adv Earth Sci 2007; 22(10): 1019–1026.

[60] Herbert TD, Ng G, Peterson LC. Evolution of Mediterranean sea surface temperatures 3.5–1.5 Ma: regional and hemispheric influences. Earth Planet Sci Lett 2015; 409: 307–318.

[61] Jiménez-Moreno G, Burjachs F, Expósito I, et al. Late Pliocene vegetation and orbital-scale climate changes from the western Mediterranean area. Glob Planet Change 2013; 108: 15–28.

[62] Capozzi R, Dinelli E, Negri A, et al. Productivity-generated annual laminae in mid-Pliocene sapropels deposited during precessionally forced periods of warmer Mediterranean climate. Palaeogeogr Palaeoclimatol Palaeoecol 2006; 235(1–3): 208–222.

[63] Lepre CJ, Quinn RL. Aridification and orbital forcing of eastern African climate during the Plio-Pleistocene. Glob Planet Change 2022; 208: 103684.

[64] Lupien RL, Russell JM, Yost CL, et al. Vegetation change in the Baringo Basin, East Africa across the onset of Northern Hemisphere glaciation 3.3–2.6 Ma. Palaeogeogr Palaeoclimatol Palaeoecol 2021; 570: 109426.

[65] Feakins SJ, DeMenocal PB, Eglinton TI. Biomarker records of late Neogene changes in northeast African vegetation. Geology 2005; 33(12): 977–980.

[66] Kroon D, Alexander I, Little M, et al. Oxygen isotope and sapropel stratigraphy in the eastern Mediterranean during the last 3.2 million years. In Proc Ocean Drill Program Sci Results 1998; 160: 181–189.

[67] Colleoni F, Masina S, Negri A, et al. Plio–Pleistocene high–low latitude climate

interplay: A Mediterranean point of view. Earth Planet Sci Lett 2012; 319: 35–44.

[68] deMenocal PB. Plio-Pleistocene African climate. Science 1995; 270(5233): 53–59.

[69] deMenocal PB. African climate change and faunal evolution during the Pliocene–Pleistocene. Earth Planet Sci Lett 2004; 220(1–2): 3–24.

[70] Ao H, Rohling EJ, Zhang R, et al. Global warming-induced Asian hydrological climate transition across the Miocene–Pliocene boundary. Nat Commun 2021; 12(1): 1–13.

[71] Qin J, Zhang R, Kravchinsky VA, et al. 1.2 Myr Band of Earth-Mars Obliquity Modulation on the Evolution of Cold Late Miocene to Warm Early Pliocene Climate. J Geophys Res Solid Earth 2022; 127(4): e2022JB024131.

[72] Van Vugt N, Langereis CG, Hilgen FJ. Orbital forcing in Pliocene–Pleistocene Mediterranean lacustrine deposits: dominant expression of eccentricity versus precession. Palaeogeogr Palaeoclimatol Palaeoecol 2001; 172(3–4): 193–205.

[73] Luo Z, Su Q, Wang Z, et al. Orbital forcing of Plio-Pleistocene climate variation in a Qaidam Basin lake based on paleomagnetic and evaporite mineralogic analysis. Palaeogeogr Palaeoclimatol Palaeoecol 2018; 510: 31–39.

[74] Caballero-Gill RP, Herbert TD, Dowsett HJ. 100-kyr paced climate change in the Pliocene warm period, Southwest Pacific. Paleoceanogr Paleoclimatol 2019; 34(4): 524–545.

[75] Wang Y, Lu H, Wang K, et al. Combined high-and low-latitude forcing of East Asian monsoon precipitation variability in the Pliocene warm period. Sci Adv 2020; 6(46): eabc2414.

[76] Popescu SM, Suc JP, Loutre MF. Early Pliocene vegetation changes forced by eccentricity-precession. Example from Southwestern Romania. Palaeogeogr Palaeoclimatol Palaeoecol 2006; 238(1–4): 340–348.

[77] Tian YY, Zhou Z, Chi CT, et al. The paleoclimate change period of the Late Pliocene-Early Pleistocene recorded by pollen from core PL02 in Yinchuan Basin. Quatern Sci 2020; 40(6): 1418–1430.

[78] Li F, Wu N. Pliocene land snail record from western Chinese Loess Plateau and implications for impacts of the summer insolation gradient between middle and low latitudes on the East Asian summer monsoon. Glob Planet Change 2010; 72(1–2): 73–78.

[79] Hansen MA, Passchier S, Khim BK, et al. Threshold behavior of a marine-based sector of the East Antarctic Ice Sheet in response to early Pliocene ocean warming. Paleoceanography 2015; 30(6): 789–801.

[80] Hopley PJ, Marshall JD, Weedon GP, et al. Orbital forcing and the spread of C4 grasses in the late Neogene: stable isotope evidence from South African speleothems. J Hum Evol 2007; 53(5): 620–634.

[81] Tiedemann R, Franz SO. Deep-water circulation, chemistry, and terrigenous sediment supply in the equatorial Atlantic during the Pliocene, 3.3–2.6 Ma and 5–4.5 Ma. In Proc Ocean Drill Program Sci Results 1997; 154: 299–318.

[82] Jansen E, Mayer LA, Backman J, et al. Evolution of Pliocene climate cyclicity at Hole 806B (5–2 Ma): oxygen isotope record. In Proc Ocean Drill Program Sci Results 1993; 130: 349–362.

[83] Medina-Elizalde M, Lea DW. Late Pliocene equatorial Pacific. Paleoceanography 2010; 25(2): PA2208.

[84] Gao P, Nie J, Breecker DO, et al. Similar magnetic enhancement mechanisms between Chinese loess and alluvial sediments from the Teruel Basin, NE Spain, and paleoclimate implications. Geophys Res Lett 2022; 49(6): e2021GL096977.

[85] Naish TR, Wilson GS. Constraints on the amplitude of Mid-Pliocene (3.6–2.4 Ma) eustatic sea-level fluctuations from the New Zealand shallow-marine sediment record. Philoso Trans R Soc A 2009; 367(1886): 169–187.

[86] Miller KG, Wright JD, Browning JV, et al. High tide of the warm Pliocene: Implications of global sea level for Antarctic deglaciation. Geology 2012; 40(5): 407–410.

[87] Grant GR, Naish TR, Dunbar GB, et al. The amplitude and origin of sea-level variability during the Pliocene epoch. Nature 2019; 574(7777): 237–241.

[88] Kaboth-Bahr S, Koutsodendris A, Lu Y, et al. A late Pliocene to early Pleistocene

(3.3–2.1 Ma) orbital chronology for the Qaidam Basin paleolake (NE Tibetan Plateau) based on the SG-1b drill core record. Newsl Stratigr 2020; 479–496.

[89] Zhao K, Du X, Jia J, et al. Effects of sea-level variation and sedimentary noise variation on the development of biogenic reefs since the Pliocene among the Xisha Islands, South China Sea. Geol Soc Am Bull 2022; 134(7–8): 1781–1792.

[90] Sun Y, Clemens SC, An Z, et al. Astronomical timescale and palaeoclimatic implication of stacked 3.6-Myr monsoon records from the Chinese Loess Plateau. Quatern Sci Rev 2006; 25(1–2): 33–48.

[91] Zhang T, Fan S, Chen S, et al. Climate change and tectonic implications during the Pliocene climate transition interval from lacustrine records in western Wei River Basin, central China. Geol J 2020; 55(11): 7385–7399.

[92] Li X, Peng T, Ma Z, et al. Late Miocene–Pliocene climate evolution recorded by the red clay cover on the Xiaoshuizi planation surface, NE Tibetan Plateau. Clim Past 2019; 15(2): 405–421.

[93] Patterson MO, McKay R, Naish T, et al. Orbital forcing of the East Antarctic ice sheet during the Pliocene and Early Pleistocene. Nat Geosci 2014; 7(11): 841–847.

[94] Vandenberghe J, Lu H, Sun D, et al. The late Miocene and Pliocene climate in East Asia as recorded by grain size and magnetic susceptibility of the Red Clay deposits (Chinese Loess Plateau). Palaeogeogr Palaeoclimatol Palaeoecol 2004; 204(3–4): 239–255.

[95] Panitz S, Salzmann U, Risebrobakken B, et al. Orbital, tectonic and oceanographic controls on Pliocene climate and atmospheric circulation in Arctic Norway. Glob Planet Change 2018; 161: 183–193.